

Interrogation of the Selectivity and Electrokinetics of CO₂ Reduction by AgSn Films in the Presence of Protic Organic [DBU–H]⁺ Cations as judged by Impedance Spectroscopy and Distribution of Relaxation Times Analysis

Thabiso Kunene, Abderrahman Atifi, and Joel Rosenthal*

Department of Chemistry and Biochemistry, University of Delaware, Newark, Delaware, 19716, USA

ABSTRACT

The use of renewable electricity to synthesize high energy and high value chemicals via reduction of CO₂ is an attractive strategy for renewable energy storage. Improving our understanding of how heterogeneous CO₂ reduction electrocatalysts function is important to designing efficient systems for conversion of CO₂ into commodity chemicals such as CO and HCO₂H. Both Ag- and Sn-based materials have been previously considered as CO₂ reduction catalysts and offer distinct CO₂RR selectivities. In this work, we have considered electrodeposited composite film electrodes prepared from electroplating baths with varying ratios of Ag⁺ and Sn²⁺ triflates to understand how the performance of such composite materials varies as a function of composition. XPS analysis confirms that for each composite film electrodes, Ag existed in the metallic (Ag⁰) state, while the Sn was mainly oxidized (Sn^{2+/4+}). The AgSn composite film electrodes studied herein are therefore best considered as AgSnO_x cathodes with varying ratios of Ag⁰:Sn^{2+/4+}. These systems were assessed as CO₂RR electrocatalysts and were found to promote the 2e⁻/2H⁺ reductions to deliver CO and HCOOH with fast kinetics and high efficiencies from electrolyte solutions containing the protic organic cation [DBU–H]⁺ (*i.e.*, protonated 1,8-diazabicyclo[5.4.0]undec-7-ene). While Sn-rich composite films showed poor selectivities for CO versus HCO₂H, a significant increase in CO versus HCO₂H selectivity (up to 99%) is achieved for composite film electrodes in which the Ag content ranged from 25 - 75%. By tuning the ratio of Ag⁰ to SnO_x we prepared composite film cathode materials that support quantitative current efficiencies for generation of CO with geometric current densities approaching 30 mA/cm² at applied overpotentials that are less than 750 mV were realized. Additionally, electrochemical impedance spectroscopy (EIS) coupled with analysis of the distribution of relaxation times (DRT) was used to better understand factors important to the composites' activity under CO₂RR conditions. Probing the dynamics with DRT analysis revealed that multiple processes relating to both adsorption and diffusion-controlled events are important to the activity of the electrocatalysts considered in this work. The collection of electroanalytical investigations suggest that synergistic interactions between Ag and SnO_x give rise to rough films that support enhanced CO₂RR kinetics and that mixing of Ag with SnO_x enhances the efficacy of adsorption and stabilization of reduced CO₂ intermediates and [DBU–H]⁺ cations to facilitate CO evolution at the cathode/electrolyte interface.

KEYWORDS: CO₂ Reduction, Electrocatalyst, Composite, Metal Oxide, Protic Ionic Liquid, Carbon Monoxide, Formic Acid

INTRODUCTION

Over last several decades, a number of strategies for mitigation of CO₂ emissions and atmospheric CO₂ concentrations have been proposed, as the development of green energy sources is one of the most pressing needs to reduce reliance on fossil fuels.¹ However, most renewable energy sources such solar and wind are intermittent and thus are not always available in sufficient quantities during periods when energy demand is highest. Accordingly, there is a great need for reliable methods to convert, store, and transport renewable energy resources such that they are available when and where they are needed. One promising strategy to store renewable energy is in the form of chemical bonds by using renewable electricity to drive the formation of chemical fuels.² An advantages of this approach is that it can be coupled to CO₂ sequestration and reduction to electrosynthesize commodity chemicals and fuel precursors. If the energy used for such transformations is generated from renewable sources, the electrochemical conversion can become a versatile method for solar energy storage.²

The electrocatalytic CO₂ reduction reaction (CO₂RR) has received major attention as a means to sustainably drive commodity chemical synthesis and for renewable energy storage. For instance, high-volume commodity chemical and fuel precursors such as carbon monoxide and formic acid can be obtained as final products from readily available inputs including electricity from a renewable sources, water and CO₂, since the electrolyte can be fully recycled with proper electrolyzer design.^{3,4} Despite the advantages associated with CO₂RR, several key thermodynamic and kinetic challenges still remain for such strategies to impact the energy landscape. Such challenges include managing the parasitic hydrogen evolution reaction (HER) that can significantly reduce the selectivity for CO₂RR under many electrolysis conditions,^{5,6} and the relatively large overpotential required to form high energy intermediates at electrode surfaces, which compromises the energy efficiency of CO₂RR schemes.^{6,7} The overall reaction kinetics are also intimately impacted by the energetics of CO₂RR intermediates for each distinct

electrocatalyst system.^{3,8} Thus, there still exists a need for the development of efficient catalytic systems for CO₂RR.

It is generally well established that all strategies to improve electrocatalytic activity should consider three main objectives, which are 1) enhancement of current density (*i.e.*, CO₂RR kinetics) at low overpotential (η) to deliver a single energy dense and/or value added product; 2) inhibition of competing reactions such as HER or other electrolyte decomposition pathways to ensure high Faradaic efficiency (FE) for the CO₂RR product of interest; and 3) the electrocatalytic system should also exhibit long-term stability in both activity and selectivity. There are several methods through which these goals can be achieved, including electrode surface modification which can be used to tune the cathode's surface properties and expose sites that may preferentially stabilize specific intermediates.⁹ Besides controlling the nature of electrode surfaces, one can also envision tuning the nature and type of proton sources for the specific proton coupled electron transfer (PCET) reactions required to deliver a specific CO₂RR product. To this end, ionic liquids and protic organic cations represent classes of electrolyte additives that can help achieve such goals based on their unique physico-chemical properties, including their negligible vapor pressures, wide electrochemical windows, and relatively high electrical conductivity, which are all advantageous for electrochemical applications.^{10,11} Furthermore, the molecular structures of ionic liquid and protic organic cations can be tuned to increase the absorption/solubility of CO₂ in electrolyte solutions,¹² which is also beneficial for CO₂RR applications.

Over the past several years, our lab has developed strategies for using imidazolium ([Im]⁺) based cations to promote CO₂RR in non-aqueous electrolyte solutions in combination with relatively inexpensive post-transition metal-based thin film cathodes.^{13,14,15} We have demonstrated that the addition of millimolar concentrations of [Im]⁺ promoters facilitates CO₂ reduction to CO at low overpotential, with selectivity exceeding FE_{CO} = 85%. By comparing the activity of monometallic thin films to their alloyed counterparts under similar electrochemical

conditions, we have demonstrated that the $[\text{Im}]^+$ promoter appears to account for the high CO selectivity and functions in conjunction with the cathode material to determine the CO_2RR onset potential and the electrode kinetics.¹⁵

Similar to controlling the pH of aqueous electrolyte solutions, use of protic organic cations or ionic liquids that are more acidic than $[\text{Im}]^+$ derivatives represent an intriguing class of ionic salts for electrochemical applications.^{16,17} It has been established that the electrolyte composition can strongly influence the outcome and characteristics of electrochemical reactions such as CO_2 reduction, and provide a means to tune the energetics of CO_2RR reaction pathways and products distributions.^{12,16,18,19,20} Therefore, besides the ability to stabilize reduced CO_2 intermediates and provide a lower energy pathway for CO_2 reduction, different types of protic organic cations can promote electrosynthesis of more reduced CO_2RR products especially those whose formation is predicted to be pH dependent.^{12,21,22} Unlike purely aqueous electrolytes, organic electrolytes containing designer organic cations can feature tunable proton availabilities while simultaneously suppressing the unwanted HER pathway. For instance, in our laboratory, we have demonstrated that in the presence of millimolar levels of a protic organic cation generated by protonation of 1,8-diazabicyclo[5.4.0]undec-7-ene ($[\text{DBU-H}]^+$ – structure shown in the Supporting Information), bismuth cathodes can rapidly convert CO_2 to formic acid with $\text{FE}_{\text{FA}} \sim 80\%$. The formic acid generating electrocatalysis observed for the $\text{Bi}/[\text{DBU-H}]^+$ system is in stark contrast to the CO evolution CO_2RR pathways that dominate for $\text{Bi}/[\text{Im}]^+$, demonstrating that bismuth cathodes display catalytic plasticity, in which the outcome of CO_2RR can be tuned through variation of the protic organic electrolyte cations that are used.²³ $[\text{DBU-H}]^+$ has also been used as a protic organic cation to promote the electrochemical reduction of NO to NH_3 by an iron porphyrin catalyst.²⁴

Amongst the transition metals, silver is one of the most promising CO_2 reduction electrocatalysts due to its relatively low overpotential and high selectivity for CO evolution.²⁵ A number of researchers have demonstrated that Ag promotes CO evolution in both aqueous and non-aqueous systems with varying electrokinetics that are largely influenced by the surface

morphology and nature of electrolyte adsorption at the electrode-electrolyte interface.^{25,26,27} It has also been shown that oxide derived nanostructured Ag materials exhibit excellent ability to convert CO₂ to CO with selectivities exceeding 80%.

Of all the post-transition metals, Sn based electrocatalysts are also some of the most intriguing CO₂ reduction electrocatalysts due to the unique surface electrochemistry of Sn that is brought on by the existence of multiple oxidation states as well as the existence of surface metal hydroxides.²⁸ In 1994 Hori et. al. demonstrated that tin electrodes could reduce CO₂ to formate albeit at high overpotentials and with just modest current densities.^{29,5} Since then, numerous studies employing Sn cathodes for CO₂ activation²⁸ have demonstrated that the ratio of CO to HCOOH production is highly dependent on the pH of the electrolyte solution. It has been suggested that formation of distinct protonated CO₂ reduction intermediates which have different stabilization energies on the Sn electrodes and can ultimately go on to deliver CO or HCOOH are sensitive to the specific pH of the electrolyte.^{30,31}

For both Ag and Sn cathodes, it has been demonstrated that the metallic and metal oxide components on the Ag and Sn surfaces contribute to the product selectivities and activities displayed by these systems, with increased levels of oxides serving to facilitate the conversion of CO₂ to formate^{32, 33,34,35, 34,36} Similar correlations have also been made for mixed AgSn cathode materials. For instance, Jiao and coworkers developed a core shell Ag₃Sn/SnO_x nanoparticle catalyst exhibiting up to 80% selectivity for HCOOH at -0.9 V vs. RHE,³⁷ which was proposed to originate from the material's lattice expansion due to oxygen vacancies on SnO_x that promote favorable binding of HCOOH selective intermediates. However, a thicker SnO_x shell negatively impacted these materials' electrical conductivity necessitating the use of relatively thin SnO_x shells for electrocatalytically competent nanoparticles.^{37,38} Notably, it has also been proposed that the presence of SnO_x species promotes stabilization of surface bound CO₂⁻ which is an intermediate that undergoes sequential PCET processes to generate CO and HCOOH.³⁹

The influence of cathodes comprised of Sn and its oxides in promoting CO₂RR has also been probed with both in-situ Raman and ATR-IR spectroscopies which have demonstrated that decreased selectivities in HCOOH production can be correlated to the reduction of SnO_x to metallic Sn.^{40,41} Further, a combination of quasi in situ XPS and operando XANES measurements showed that the electrodeposition of SnO_x on O₂-plasma treated Ag surfaces leads to increased stability of catalysts with suppressed HER activities and which generate CO and HCOOH from CO₂.⁴² These catalysts also exhibited increased surface roughness and hence low overpotential for CO and HCOOH evolution. While the CO₂RR activity of Ag and Sn cathodes, as well as Ag materials coated with a layer of SnO_x has been considered, the variable electrocatalytic activity afforded by composite electrocatalysts containing well defined ratios of Ag and Sn has not been thoroughly evaluated. Accordingly, such systems represent an intriguing platform to probe and evaluate potential synergistic interactions between the AgSn cathode composition along with interactions with complex electrolyte components such as protic ionic liquids.

To this end, we have considered how the [DBU-H]⁺ protic organic cation influences the outcome of CO₂RR at electrodeposited AgSn films of varying Ag/Sn composition. These systems were chosen because monometallic cathodes comprised of either Ag or Sn display completely disparate selectivities for CO₂ reduction and have been shown to form stable intermetallic compounds at room temperature that span the full range of Ag/Sn ratios. By noting how selectivity and kinetics of CO₂RR vary as a function of the Ag/Sn ratio, we have sought to understand how the AgSn composition influences the outcome of CO₂RR. In addition, by combining voltammetry and electrochemical impedance spectroscopy, we also have sought to evaluate how the AgSn cathode surface composition, and the cathodes' interactions with the [DBU-H]⁺ containing electrolyte, influence the distinct 2e⁻/2H⁺ CO₂RR pathways to deliver either CO or HCOOH.

EXPERIMENTAL SECTION

Materials and Reagents

The protic organic cation [DBU-H]PF₆ was prepared using a previously published procedure and is detailed in the Supporting Information.²³ Acetonitrile (MeCN, 99.9%) was purchased from Fisher Chemicals. Silver trifluoromethanesulfonate (Ag(OTf), 99.999%) and Tin trifluoromethanesulfonate Sn(OTf)₂, 99.99% were purchased from Matrix Scientific and TCI America, respectively. Tetrabutylammonium hexafluorophosphate ([TBA]PF₆, 98%) was purchased from TCI America and recrystallized from boiling ethanol prior to use. Purity was confirmed by ¹H and ¹³C NMR, as well as by in house CHN analysis. Carbon dioxide (CO₂, Ultra High Purity) was purchased from Keen Compressed Gas Company.

Electrochemical Methods

Voltammetry experiments were performed using a traditional three-electrode configuration and a CH Instruments CHI760D bipotentiostat. All electrochemical experiments except controlled potential electrolysis (CPE) experiments were performed in a one compartment cell using a leak-less Ag/AgCl (1.0 M KCl, CH Instruments) reference electrode calibrated with Cc/Cc⁺ (Cc = cobaltocene) as an internal standard to account for the possibility of reference drift. The counter electrode was a piece of platinum mesh (Sigma-Aldrich). CPE experiments were performed in a two-compartment cell in which the cathode and anode compartments were separated by a proton permeable nafion membrane (Nafion 212, Fuel Cell Earth).

Electrodeposition of Ag, Sn and AgSn Thin Films

The Ag, Sn and AgSn composite thin films were electrodeposited on nickel disk electrode (0.072 cm², BASI). The nickel electrodes were polished with slurry of 0.3 and 0.05 μm alumina powder in Millipore water and rinsed sequentially with water and MeCN. The electrodeposition bath consisted of 100 mM [TBA]PF₆ in MeCN containing varying amounts of the corresponding Ag(I) and Sn(II) triflate salts under N₂ saturated. The electrode substrates were not pre-conditioned before use, and galvanostatic electrodeposition was performed at 2.6 mA/cm for 10

minutes in a quiescent solution. The total concentration of metal triflates in the solution was maintained at 20 mM. The thin film electrodes that were obtained were then rinsed extensively with MeCN and dried under a stream of N₂ before use.

Linear Sweep Voltammetry

Linear sweep voltammograms were recorded in a one-compartment cell with three-electrode configuration in CO₂ saturated MeCN that had first been de-aerated by N₂ bubbling for 20 minutes. The electrolyte solutions contained 100 mM [TBA]PF₆ as well as 100 mM of [DBU–H]PF₆. A constant stream of CO₂ was maintained above the solution during all voltammetry experiments. Before electrochemical characterization of CO₂RR, the thin-film electrodes were preconditioned in a separate electrolyte solution by sweeping the potential from –1V to –1.35V vs. Ag/AgCl for at least 10 cycles. For all electrodes, the measured current was normalized by the geometric surface area. Automatic IR compensation was applied for all voltammetry measurements.

Controlled Potential Electrolysis

Controlled potential electrolysis (CPE) experiments were performed in a gas-tight, two-compartment cell separated by a Nafion membrane (NRE-212, Fuel Cell Earth). Similar to voltammetry experiments, the electrolyte solution consisted of 100 mM [TBA]PF₆ and 100 mM of [DBU–H]PF₆ in MeCN. The catholyte solution was saturated with CO₂ for at least 20 minutes and a steady flow of CO₂ was maintained over the headspace at 5 sccm throughout the course of each experiment. Both compartments of the electrolysis cell were continuously stirred at 700 RPM. The cathode headspace outlet was connected directly to the sampling loop of a gas chromatography system (SRI-8610C) equipped with a HayeSep D column and a packed Molecular Sieves 13X column. The volatile products were analyzed periodically, and solution

products were analyzed by NMR after a 2 hr experiment and quantified with reference to 1 mM dichloromethane standard in the sample NMR tube.

Electrochemical Impedance Spectroscopy

The electrode roughness was estimated using electrochemical impedance spectroscopy in quiescent N₂ saturated MeCN solutions containing 100 mM KPF₆ in the frequency range of 10000 – 100 Hz at $E = -0.225$ V vs. Ag/AgCl for the AgSnOx composites or $E = -0.775$ V vs. Ag/AgCl for the Ag-only film, which are close (within ~20 mV) to the open circuit potentials recorded under similar electrolyte conditions. Since KPF₆ is a weakly coordinating salt and soluble in MeCN it is unlikely to induce charge transfer reactions that may convolute the measurement of the double layer capacitance as is common with ammonium salts such as [TBA]PF₆.⁴³ The electrode roughness was estimated from the double layer capacitance using a modified Randles circuit adapted from the literature.^{44,45}

EIS data collected under CO₂RR conditions in the presence of [DBU-H]PF₆, were measured using similar electrolyte compositions as those employed for the voltammetry experiments in the potentiostatic mode in the frequency range of 10 kHz – 10 Hz. The Distribution of Relaxation Times (DRT) were calculated using DRTTOOLS, which is freely available software that is implemented in MATLAB code.⁴⁶ For computation of DRT spectra, an inverse quadratic function was chosen for radial basis function discretization, both real and imaginary parts of the impedance spectroscopy data were used; the regularization parameter, lambda was set to 10⁻⁴. All inductive data were ignored. All EIS data points below 10 Hz and/or exhibiting Warburg diffusion like behavior on the Nyquist plots were removed as suggested in the literature implementation of the DRT technique. The first order derivative was used as the penalties for the regularized regression and for shape control, the coefficient for the full width at half maximum (FWHM) was set to 0.5. The gaussian functions for the DRT spectra were fitted with Origin 2019

Software (OriginLab Corp.). Before DRT calculation, the EIS data were checked for linearity using well established Kramers-Kronig relationships implemented in the software Lin-KK Tool.^{47,48,49}

Surface Characterization Using X-ray Photoelectron Spectroscopy

All XPS analysis was conducted using a Thermo Scientific K-alpha instrument using an Al-K α Xray source with a flood gun. For high resolution XPS, 10 scans were averaged with a spot size of 400 μm , pass energy of 50 eV, dwell time of 50 ms and a step size of 0.1 eV. A Shirley type background was subtracted from all XPS spectra and the binding energy for all XPS spectra were corrected for shift with reference to the C 1s binding energy set to 284.8 eV.⁵⁰

RESULTS AND DISCUSSION

Electrodeposition of Ag-Sn Oxides on Nickel Substrates

Inspection of the Ag-Sn phase diagram shows the room temperature stability of several intermetallic compounds suggesting that electrodeposition of several heterogenous Ag-Sn films is feasible,^{51, 52} however, it can be challenging to find electrolyte compositions suitable to electrodeposit films across a wide composition that all feature a homogeneous surface composition. A challenge to electrodeposition of AgSn-containing intermetallics is the need to reduce Sn⁴⁺ to Sn⁰, which is difficult because Ag⁺ is immediately reduced to Ag⁰ at much more positive potentials. Furthermore, electrodeposition of AgSn-containing phases must be performed under an inert atmosphere (e.g., N₂) since O₂ promotes the solution phase galvanic reaction whereby Ag⁺ is reduced by Sn²⁺ to form Ag metal nanoparticles with cogeneration of Sn⁴⁺ ions. This reaction is evidenced by the formation of a reddish-brown solution accompanied by the precipitation of small black particles in oxygen rich electrolytes containing Ag⁺ and Sn²⁺.

Based on the above, we galvanostatically electrodeposited several AgSn-containing phases from electroplating baths containing varying ratios of Ag(OTf) and Sn(OTf)₂ on nickel substrates at a constant current density of $j = 2.6 \text{ mA/cm}^2$ for 10 minutes. Figure 1 shows the cyclic voltammograms (CVs) obtained using a nickel disk working electrode in electrolyte

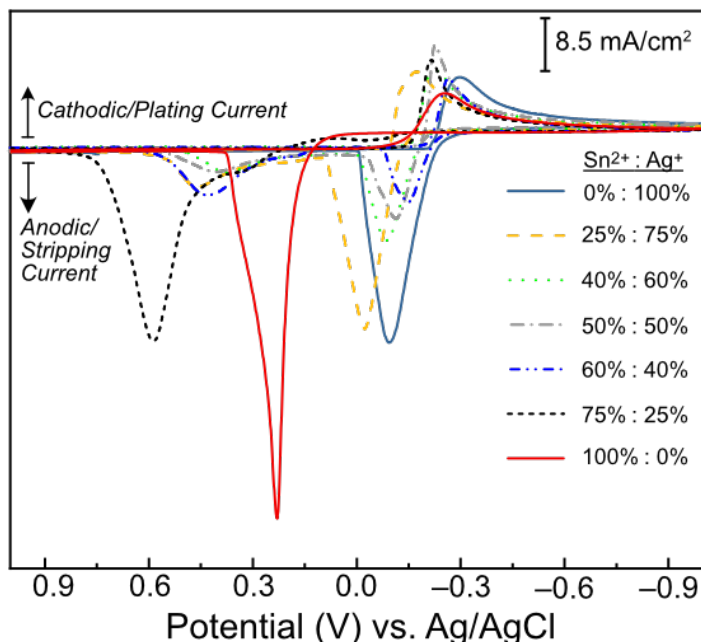


Figure 1. Representative cyclic voltammograms recorded at 100 mV/s in MeCN containing 0.1 M [TBA]PF₆ and varying ratios of Ag(OTf) and Sn(OTf)₂. The total concentration of Ag⁺ + Sn²⁺ in the solution was maintained at 20 mM. Peak potentials for a given bath composition were found to vary in any given experiment by ~5 mV. Current densities associated with plating and stripping waves varied by less than 5% per run.

solutions containing varying ratios of Ag⁺ and Sn²⁺ triflate salts in MeCN with 0.1 M [TBA]PF₆ as supporting electrolyte. The total concentration of Ag⁺ + Sn²⁺ in the solution was maintained at 20 mM, with specific ratios of Ag/Sn as shown in Figure 1. The total ionic strength was kept constant for each solution in order to limit its influence on the observed current density. Waves for AgSn co-deposition and stripping vary as a function of the electrolyte composition. The voltammograms indicate that as the relative amount of Ag⁺ increases from 25–75%, the peak plating potential remained constant at approximately –0.2 V vs. Ag/AgCl. However, within this same regime, the peak stripping potentials differ significantly and shift more positively with increasing amounts of Ag⁺ ions in solution. The scans that sweep to positive potentials also exhibit two peak waves that can be attributed to the presence of multiple species on the films formed during the reductive scans.

Interestingly, the Ag⁺ and Sn²⁺ reduction peaks begin to merge in the presence of Sn²⁺ ions, which may indicate a homogenous reaction between Ag⁺ and Sn²⁺ that results in the

deposition of a single species. With increasing Ag^+ concentration, the peak current of the anodic waves also changes significantly. The current density of the first peak decreases from approximately -12.9 mA/cm^2 to -8.6 mA/cm^2 whereas the current density of the second anodic peak increases from -4.3 mA/cm^2 up to -30 mA/cm^2 . It is noteworthy that the observed peak positions for the stripping potentials are significantly different from those recorded from electrolytes containing either only $\text{Ag}(\text{OTf})$ or only $\text{Sn}(\text{OTf})_2$. The appearance of additional peaks between those of the pure metal films is a characteristic feature observed for electrooxidation of metastable intermetallic crystal phases.⁵³

Surface Characterization

X-ray photoelectron spectroscopy (XPS) measurements were carried out to determine the surface composition of each of the AgSn composite film electrodes. Figures 2 and S1 show representative high resolution XPS spectra in the Ag and Sn region of the Ag-Sn composites and the films that contain either only Ag or Sn. All XPS spectra were calibrated to the C 1s peak set to 284.8 eV.⁵⁰ The high resolution Sn 3d region shows multiple peaks that were fitted to three

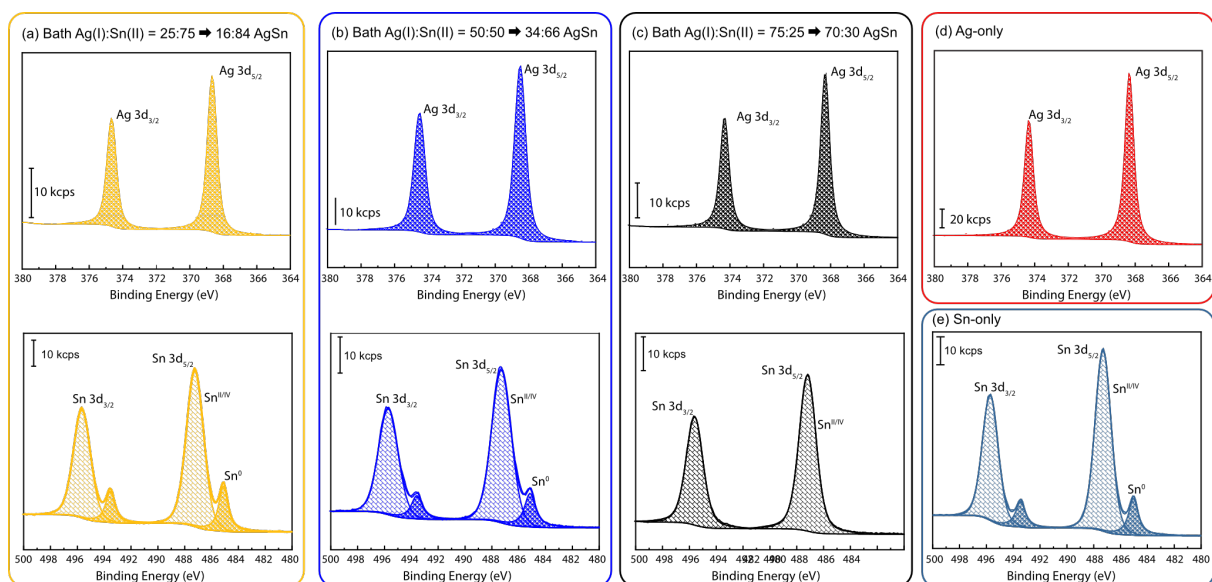


Figure 2. Representative high-resolution XPS spectra showing the Ag and Sn regions for various as electrodeposited AgSn composite films, as well as monometallic Ag- and Sn-based films. Representative spectra are shown for thin film electrodes prepared from electrodeposition baths with the following ratios of Ag(I) and Sn(II) triflate salts: (a) 25:75; (b) 50:50; (c) 75:25; (d) 100:0; and (e) 0:100. The total concentration of metal triflate salts in all electrodeposition baths was 20 mM.

components corresponding to Sn^0 , and oxidized $\text{Sn}^{2+} + \text{Sn}^{4+}$ species. The surface composition of each electrodeposited film was determined independently using a similar peak deconvolution

Table 1: The surface Ag/Sn atomic ratio determined by XPS analysis in comparison to the electrodeposition bath composition.

Electroplating Bath Ratios ($\text{Ag}^+:\text{Sn}^{2+}$)	Electrode Surface Composition of Tin and Silver ^a	
	Tin (%)	Silver (%)
(0:100)	100	0
(25:75)	84	16
(40:60)	76	24
(50:50)	66	34
(60:40)	47	53
(75:25)	30	70
(100:0)	0	100

^aAtomic ratios are accurate to within $\pm 2\%$ based on XPS analyses shown in Figure 2.

procedure, whereby the high-resolution Sn 3d XPS region was fit with two components corresponding to Sn^0 , and oxidized $\text{Sn}^{2+/4+}$.⁵⁰

Based on the XPS data shown in Figures 2 and S1, we were able to determine the ratio of all surface Ag species versus all surface Sn species on the film electrodes, as a function of the electroplating bath composition. These data are compiled in Table 1 and in Figures 3 and S2. The

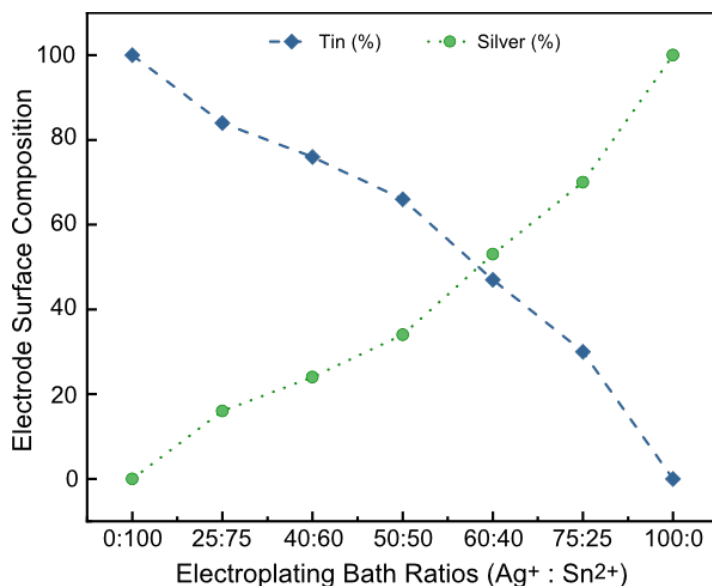


Figure 3. Representative levels of Ag and Sn on the surface of the electrodeposited film electrodes as a function of the ratio of Ag^+ and Sn^{2+} in the electroplating bath

data indicate that the relative ratios of electrodeposited Ag versus Sn is sensitive to the composition of the electroplating bath, but that the amount of surface Sn species is generally slightly higher than what might be expected based on the ratio of $\text{Ag}^+:\text{Sn}^{2+}$ in solution during plating. The lower surface silver content could be due to the competing solution phase galvanic reduction of Ag^+ to insoluble Ag^0 by the Sn^{2+} cations, as discussed above. This background galvanic process may be expected to attenuate the amount of Ag^+ available for deposition at the electrode surface. Such an effect would be compounded by electrodeposition under quiescent conditions. We note, that it is also possible that monolayers of Ag are initially electrodeposited on the nickel substrate which then become buried beneath the bulk AgSnO_x composite film that is ultimately plated. Such a process could also result in the lower-than-expected Ag surface concentration that we observe for the composite films.

While for each of the films, silver exists exclusively in the metallic state (Ag^0), all of the AgSn composites and the Sn-only film show a preponderance of surface $\text{Sn}^{2+/4+}$ (as opposed to metallic Sn^0). The average percentages of metallic versus oxidized Sn species are presented in Table 2 indicating that all of the Sn containing films contain surface $\text{Sn}^{2+/4+}$ species. Overall, the metallic Sn^0 is a minor component of all tin-containing films. Oxidized $\text{Sn}^{2+/4+}$ is the dominant surface oxidation state for all the tin-containing films and hovers around 85-90%. Accordingly, the surface composition of the electrodeposited materials are best described as AgSnO_x composite films.

Table 2: Relative percentages of metallic Sn^0 versus oxidized $\text{Sn}^{2+/4+}$ at the surface of the electrodeposited films considered in this study.

Electroplating Bath Ratios ($\text{Ag}^+:\text{Sn}^{2+}$)	Sn^0	$\text{Sn}^{2+/4+}$
(0:100)	10%	90%
(25:75)	13%	87%
(40:60)	11%	89%
(50:50)	16%	84%
(60:40)	13%	87%
(75:25)	0%	100%
(100:0)	—	—

Relative Surface Roughness

The relative electrochemical surface area (ECSA) for each AgSnO_x electrode can be estimated from the electrochemical double layer capacitance of the electrode-electrolyte interface in a non-adsorbing electrolyte such as KPF₆ in MeCN.⁴³ Due to the presence of SnO_x on the electrode surfaces, the common method of measuring the doubling layer capacitance via voltammetry is unsuitable due to the propensity for surface Sn oxides to undergo reduction. Therefore, we chose to measure the frequency dependent impedance of the same electrode-electrolyte system using electrochemical impedance spectroscopy (EIS). The electrolyte for impedance measurements consisted of 100 mM KPF₆ in N₂ saturated MeCN and the chosen frequency for EIS experiments varied from 100 – 10,000 Hz. The EIS measurements were performed under potentiostatic mode with the potential held at $E = -0.225$ V vs. Ag/AgCl for AgSnO_x composites or $E = -0.775$ V vs. Ag/AgCl for the Ag-only film. We note that these potentials are close to the open circuit potentials for these films under the electrolyte conditions employed for the impedance measurements. The EIS data we obtained (Figure 4a) were fit to a

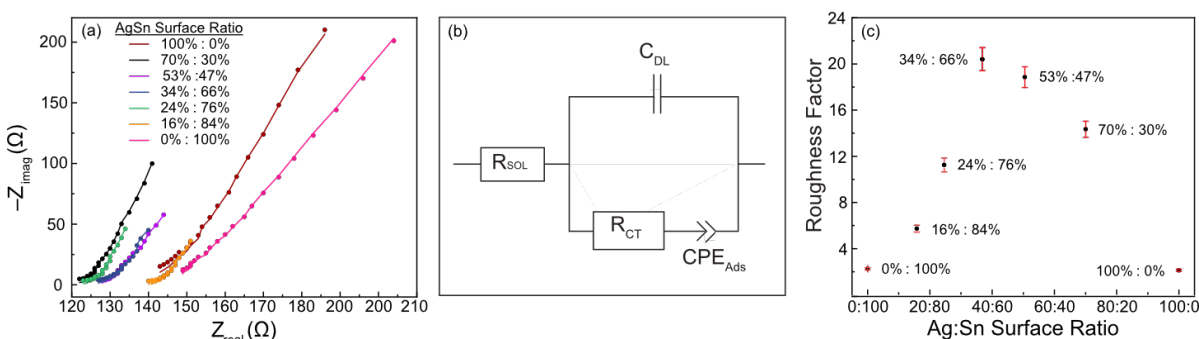


Figure 4. Double layer capacitance measurements for determining the relative surface Roughness Factors for electrodeposited AgSn electrodes. (a) Nyquist plots constructed for EIS data recorded for electrodeposited AgSn composite films in 100 mM KPF₆ in MeCN at -0.225 V vs. Ag/AgCl. The solid lines are data simulations generated using the modified Randles equivalent electrical circuit that is shown in panel (b). The parameters associated with adsorbed ionic species on the electrode are represented by R_{ct} and CPE_{ads} connected in parallel to the double layer capacitance C_{dl} . R_{ct} is an adsorption resistance, and CPE_{ads} is the constant phase element to model the adsorption of electrolyte components on the electrodes surface. (c) Plot of the relative surface roughness versus a bare nickel electrode as a function of the electrode surface composition.

modified Randles circuit (Figure 4b) consisting of an R_{sol} element (electrolyte resistance) as well as a parallel combination of a capacitor and resistor representing the electrode-electrolyte double layer.^{44,45} An additional constant phase element (CPE) is included in series with the R_{ct} element to model a pseudo-capacitive contribution of the SnO_x reduction as well as electrolyte adsorption.

In order to compare the intrinsic properties of the electrodes, the surface Roughness Factor of each electrode was calculated using Equation 1. Consideration of the relative surface roughnesses of each of the thin film electrodes is relatively convenient and allows us to compare the activity of the different electrodeposited thin films to one another, while normalizing for differences in ECSA.

$$Roughness\ Factor = \frac{C_{Film}}{C_{Nickel}} \quad (Eq. 1)$$

The surface Roughness Factor for each thin film was determined by comparing the double-layer capacitance for each of the electrodeposited films (C_{Film}) to that of a smooth and planar bare nickel electrode (C_{Nickel}) onto which the films were deposited. All double layer capacitance measurements were performed using freshly deposited thin films in fresh electrolyte solutions to avoid electrode contamination. Figure 4c indicates that the roughness of the films increased linearly with Ag content up to about 50% mixtures of Ag and Sn, after which the roughness decreases uniformly. Relative surface roughnesses for each of the composite films are tabulated in Table S1.

AgSn Composite Films as Electrocatalysts for CO₂RR

The electrocatalytic activity of each of the film electrodes was probed by linear sweep voltammetry (LSV) using a standard three-electrode configuration in a one-compartment electrochemical cell. Voltammetric analysis was performed at a scan rate of $\nu = 100$ mV/s in CO₂ saturated MeCN containing 100 mM [TBA]PF₆ and 100 mM [DBU-H]PF₆. Before each LSV was recorded, the film electrodes were preconditioned in the same electrolyte solution to remove

nonspecifically adsorbed metal particles and ensure surface homogeneity. Representative linear sweep voltammograms recorded for Ag-only, Sn-only, and AgSnO_x composite films are shown in Figure 5a.

Analysis of the LSVs in Figure 5a reveals that the AgSnO_x composite films have onset potentials for CO₂ reduction that are shifted *positively* relative to the Ag-only and Sn-only films. Even the incorporation of relatively small amounts of Ag into the composite films (e.g. ~25% Ag, Figure 5a, orange trace) shifts the resulting voltammogram for CO₂RR to more positive onset potentials than for either the Ag- or Sn-only films. The shift to more positive potentials continues with increased Ag content, with the least negative onset potentials for CO₂ activation being observed for composite films that were electrodeposited from solutions that contained Ag⁺ and Sn²⁺ triflates in a 3:1 ratio. Based on the XPS analyses compiled in Table 1, these represent AgSnO_x composite films with surface compositions that feature Ag:Sn in a 7:3 ratio. The variable onset potentials observed for each of the thin films probed for CO₂RR may in part reflect the increased surface roughnesses of the composite films relative to those of the Ag- and Sn-only electrodes (Figure 4c, Table S1).

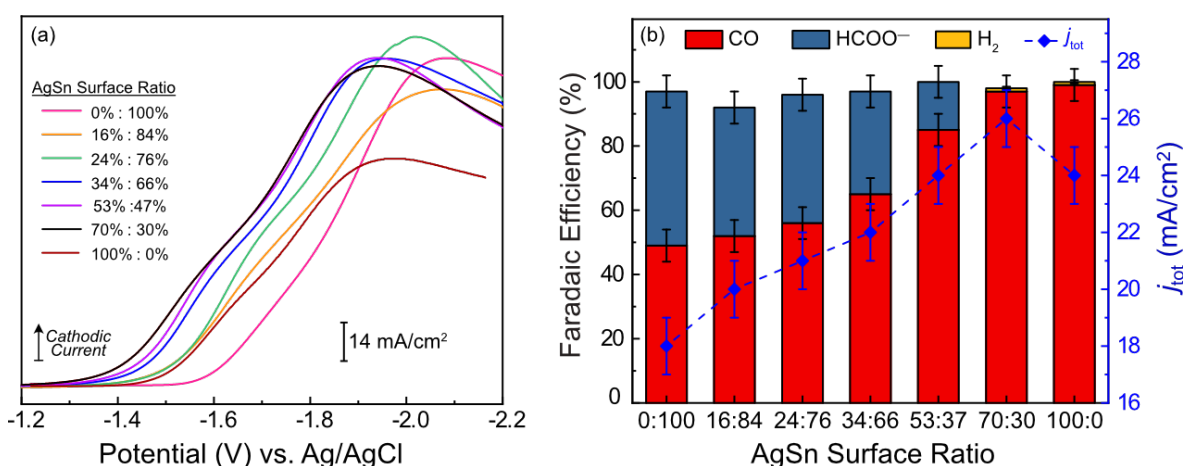


Figure 5. (a) Linear sweep voltammograms (LSVs) recorded for electrodeposited Ag, Sn, and composite AgSn films in CO₂ saturated MeCN solutions containing 100 mM [TBA]PF₆ and 100 mM [DBU-H]PF₆. (b) Faradaic efficiencies for generation of CO, formate, and H₂, as well as total geometric current density for CO₂RR using Ag, Sn, and composite film electrodes. CPE experiments were performed at -1.85V vs. Ag/AgCl for 2 hours in MeCN based electrolyte solutions containing 100 mM [TBA]PF₆ and 100 mM [DBU-H]PF₆.

Table 3. Electrocatalysis metrics recorded for the Ag, Sn, and composite film electrodes.^a

Electrode Film Ratio Ag:Sn Ratio	FE _{FA}	FE _{CO}	FE _{H₂}	j _{tot} (mA/cm ²)
0:100 (Sn-only)	48 ± 2	49 ± 2	—	18 ± 1
16:84 AgSn	40 ± 2	52 ± 3	—	20 ± 1
24:76 AgSn	40 ± 2	56 ± 3	—	21 ± 1
34:66 AgSn	32 ± 1	65 ± 3	—	22 ± 1
53:47 AgSn	15 ± 1	85 ± 4	—	24 ± 1
70:30 AgSn	—	97 ± 5	1 ± 0.5	26 ± 1
100:0 (Ag-only)	—	99 ± 5	1 ± 0.5	24 ± 1

^aCPE experiments were performed at -1.85 V vs. Ag/AgCl for 2 hours in MeCN based electrolyte solutions containing 100 mM [TBA]PF₆ and 100 mM [DBU-H]PF₆.

To investigate the electrocatalytic performance of the electrodeposited films, controlled potential electrolysis (CPE) experiments were performed at -1.85 V vs. Ag/AgCl over the course of 2 hours in MeCN based electrolyte solutions containing 100 mM [TBA]PF₆ and 100 mM [DBU-H]PF₆. Under these conditions, the Ag-only and Sn-only cathodes support distinct electrocatalysis (Figure 5b, Table 3). The Ag/[DBU-H]⁺ electrocatalyst system is quantitatively selective for the $2e^-/2H^+$ reduction of CO₂ to CO (FE_{CO} = 99%), with relatively fast kinetics of $j = 24$ mA/cm². By contrast, the Sn/[DBU-H]⁺ system shows roughly equal selectivity for both $2e^-/2H^+$ reductions of CO₂ to generate CO and HCO₂H (FE_{CO} = 49%, FE_{FA} = 48%), with overall CO₂RR kinetics ($j = 18$ mA/cm²) that are approximately 25% slower than those displayed by the Ag/[DBU-H]⁺ system. The lower current density observed for the Sn-only thin film is expected based on the voltammetry in Figure 5a, since this cathode material displays the most negative onset potential for CO₂RR. The differences in electrocatalytic performance of Ag versus Sn have been observed previously and can be ascribed to the adsorption energies of key intermediates such as CO₂⁻, COOH and O₂CH which are dependent on the identity of the metal electrode.^{7,28,29}

The CO₂RR selectivity profiles displayed by the composite AgSnO_x films is closer to that of the Sn-only cathode up to films whose surface composition is approximately 66% Sn (34% Ag) based on XPS analysis (Figure 5b, Table 3). Although initially the CO₂RR selectivity does not change markedly as the percentage of Ag is increased in the Sn films, the kinetics for CO₂RR

undergo a clear enhancement of nearly 20% (Figure 5b, Table 3) as up to 34% Ag is added to the composite films. Although the films containing approximately 66% and 50% Sn do show enhanced selectivity and kinetics for CO evolution relative to the Sn-only cathode, their activity is unstable over the course of a 2-hour electrolysis suggesting that their surface composition or morphology may evolve during the CPE (Figure S3). Nonetheless, within the first 2 hours of electrolysis at $E_{appl} = -1.85$ V, the selectivity for CO evolution shows a nearly linear dependence on the film surface composition (Figure 5).

Of all the composite films that were evaluated for CO₂RR, the film consisting of ~70% Ag, displayed the most positive onset potential and also selectively evolves CO gas with little to no HCO₂H or H₂ production. Accordingly, the composite electrode with surface composition of 70% Ag displayed FE_{CO} values that are virtually identical to the Ag-only cathode but operates with the fastest kinetics of all the systems considered in this study. Accordingly, the composite film comprised of AgSn in a 70:30 ratio represents the most attractive cathode considered in this study as it supports the fastest kinetics for CO₂RR of all the systems evaluated and is selective for conversion of CO₂ to CO (FE_{CO} = 97%).

The Sn 3d XPS spectra (Figures 2 and S1) recorded for the AgSnO_x composite films provide evidence for the presence of oxidized surface Sn^{2+/4+} species in those cathode materials. The presence of highly oxidized Sn species has also been suggested to be responsible for enhanced selectivity and activity towards promoting CO₂ reduction rather than HER in a number of aqueous CO₂ reduction systems.^{54,55} For instance, Kanan and coworkers have demonstrated that metallic tin promotes H₂ evolution whereas oxidized Sn foil promotes CO₂RR to deliver HCOO⁻ with greater than 90% current efficiency.³⁹ When coupled with the relatively low proton availability of the MeCN-based electrolyte solutions used in this study (pK_a of [DBU-H]⁺ ~ 24 in MeCN), it is perhaps not surprising that HER is not observed as a parasitic side reaction to any significant extent for the AgSn composites.^{39,54,55}

Origin of High Activity in Ag-doped AgSnO_x thin Films – Kinetics of Charge Transfer: Electrochemical Impedance Spectroscopy

To probe the origin of the enhanced electrocatalytic performance of the AgSnO_x composite films we performed EIS measurements in the frequency range of 10 kHz – 10 Hz at $E = -1.85$ V with an AC perturbation amplitude of 10 mV. The choice of an equivalent electrical circuit to fit EIS data usually requires a priori knowledge of the impedance behavior of the system under study.⁵⁶ However, using the Distribution of Relaxation Times (DRT) technique, the EIS data which is a function of frequency can be converted into a probabilistic distribution of the relaxation times for each process involved in the electrochemical process.^{57, 58,59} Due to the complexity of the EIS Nyquist plots (especially the curvature toward the high and low frequency limits of the experiments) obtained under CO₂RR conditions for the thin-films considered in this work (Figure S4), DRT analysis was performed to help interpret the impedance results.⁴⁶

Briefly, DRT analysis is a mathematical deconvolution that identifies the relaxation time constant distribution of the impedance data. The frequency dependent impedance in DRT is calculated by fitting the EIS data at various frequencies using the following equation.

$$Z_{DRT}(f) = R_{\infty} + \int_{-\infty}^{\infty} \frac{\gamma(\ln\tau)}{1 + i2\pi f\tau} d\ln\tau \quad (\text{Eq. 2})$$

In Equation 2, R_{∞} represents the solution resistance and $\gamma(\tau)$ is a function that describes the characteristic relaxation time constants for the electrochemical system being studied. The integration function describes the total polarization resistance of the electrochemical system and the DRT analysis affords various time or frequency dependent peaks representing the individual resistances associated with specific electrochemical events such as charge transfer or potential dependent generation/adsorption of intermediates which are characteristic for electrocatalytic processes.⁴⁶ The term τ represents the time constant and f is the frequency, respectively.

Compared to common representations of EIS data such as Nyquist plots, DRT analysis makes it easier to clearly show the different relaxation events contributing to the total impedance of the system under study, particularly in cases where these processes overlap. Furthermore, DRT analysis can be used to help guide development of an equivalent circuit to model the

experimental impedance data. For in depth discussion of the DRT analysis and the underlying theory, interested readers are referred to the primary literature detailing the development and implementation of these methods.^{46, 57, 58,59}

The mechanism of electrocatalytic CO₂ reduction is expected to involve three major physicochemical processes, which include (1) the diffusion of reactants, products, and other electrolyte components to/from the electrode surface; (2) adsorption of reactants at the polarized electrode; and (3) multiple proton-coupled charge transfer steps that ultimately drive the CO₂RR processes. In addition, for electrocatalysis conducted using electrodeposited films (as is the case for this study), one also anticipates a fourth relaxation processes relating to the ohmic contacts between the catalyst film and the underlying substrate, or between individual particles that comprise the film, especially at higher frequencies.

As shown in Figure 6, the DRT spectra indicate that within the frequency range of interest, there are three main regions with distinct distributions of relaxation times that provide information about the kinetics of charge transfer at the electrode potentials relevant to CO₂RR. Since the 70:30 AgSnO_x composite film exhibited the fastest kinetics (and lowest onset potential) for CO₂RR, its calculated DRT results were compared to the Ag-only and Sn-only films. In this study the relaxation events in the DRT spectra of Figure 6 are correlated to several physicochemical processes as follows: τ_1 (red) - Ohmic contact between the thin film and the nickel substrate; τ_2

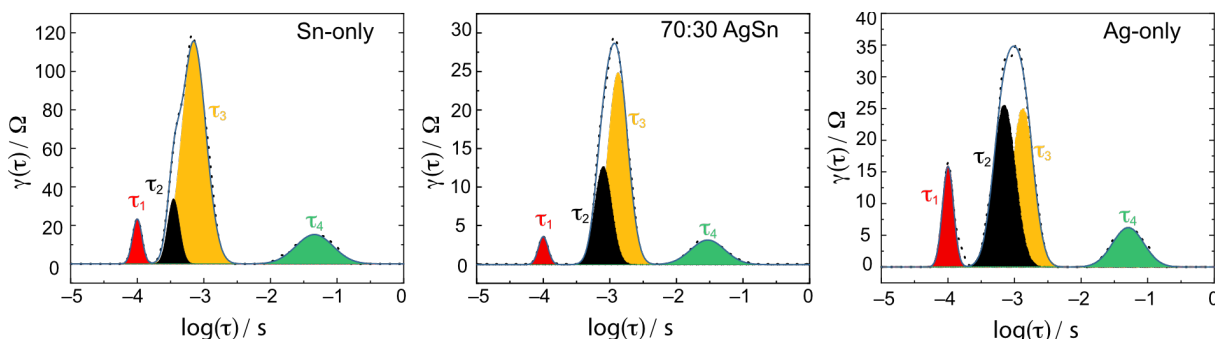


Figure 6. Distribution of Relaxation Times (DRT) plots for Ag-only, Sn-only, and 70:30 AgSn composite film electrodes measured at -1.85V vs. Ag/AgCl in CO₂ saturated MeCN containing 100 mM [DBU-H]PF₆ and 100 mM [TBA]PF₆. The colors represent relaxation events with different time constants that contribute to overall impedance during CO₂ reduction: τ_1 (red) - Ohmic contact between the thin film and the nickel substrate; τ_2 (black) - Adsorption of electrolyte ions and related intermediates; τ_3 (yellow) - Charge transfer kinetics and τ_4 (green) diffusion/capacitive behavior related to mass transport.

(black) – Surface adsorption of CO₂ and electrolyte components and related intermediates; τ_3 (yellow) - Charge transfer kinetics; and τ_4 (green) diffusion/capacitive behavior related to mass transport. The exact nature and dependence of these processes on experimental conditions relevant to electrocatalytic CO₂ reduction is still under investigation in our lab.

The DRT plots shown in Figure 6, show the resistance associated with each relaxation process with specific time constants. The first relaxation process (τ_1) is related to the ohmic contact between the electrodeposited film and the nickel substrate. This relaxation process is also related to the interparticle contact resistance in the bulk film. Depending on the electrodeposition conditions such as bath composition and applied current, each of the three film cathodes subjected to DRT analysis may have different or mixed phases. Therefore, the surface composition, morphology, phase, and thickness features of the catalyst can be factors that affect the associated resistance. The processes τ_2 and τ_3 are related to formation of an adsorbed layer of [TBA]⁺ and [DBU-H]⁺ electrolyte cations at the electrode surface, and the associated resistance of charge transfer that drives CO₂ activation, respectively. Lastly, relaxation process τ_4 is related to mass transport-controlled processes such as the diffusion of reactants to and products from the electrochemical double layer. A summary of the values of the calculated DRT spectra corresponding to the kinetics of CO₂ reduction on the Ag-only, Sn-only, and 70:30 AgSn composite films are shown in Table 4.

In an effort to evaluate the role of surface composition on the kinetics and mechanism of electrocatalytic CO₂RR, the nature of the impedance relaxation processes was probed as a function of the applied potential for the most active cathode of Figure 5b (*i.e.*, the 70:30 AgSnO_x

Table 4. Values of the DRT spectrum parameters corresponding to the kinetics of CO₂RR on Ag-only, Sn-only, and 70:30 AgSnO_x composite film electrodes as calculated from the DRT plots in Figure 6.

	τ_1	τ_2	τ_3	τ_4
Electrode	$R_1 (\Omega)$	$R_2 (\Omega)$	$R_3 (\Omega)$	$R_4 (\Omega)$
SnO _x	22	35	115	15
75AgSnO _x	7.5	9	23	2.5
AgO _x	16	26	26	6

composite film electrode). EIS measurements were recorded under the same electrolyte conditions as for the CPE experiments. Potentiostatic EIS data were collected at -1.55 V, -1.65 V, -1.75 V, and -1.85 V vs. Ag/AgCl (see associated Nyquist plots in Figure S5). As shown in Figure 7, the DRT spectra indicate that the number of discrete relaxation process do not change within the studied potential range, however, upon deconvolution of the DRT through gaussian fitting, it becomes clear that the contribution of each impedance process does change significantly as a function of the potential. Since the potential dependent DRT calculations are performed under the same electrode conditions, the relaxation process τ_1 , remains at a constant position and total resistance over the entire potential range considered (see Figure 7 and Table 5).

The processes τ_2 and τ_3 (which are the most prominent features in the DRT spectra) show a clear trend as a function of applied potential. At more negative potentials, these time constants

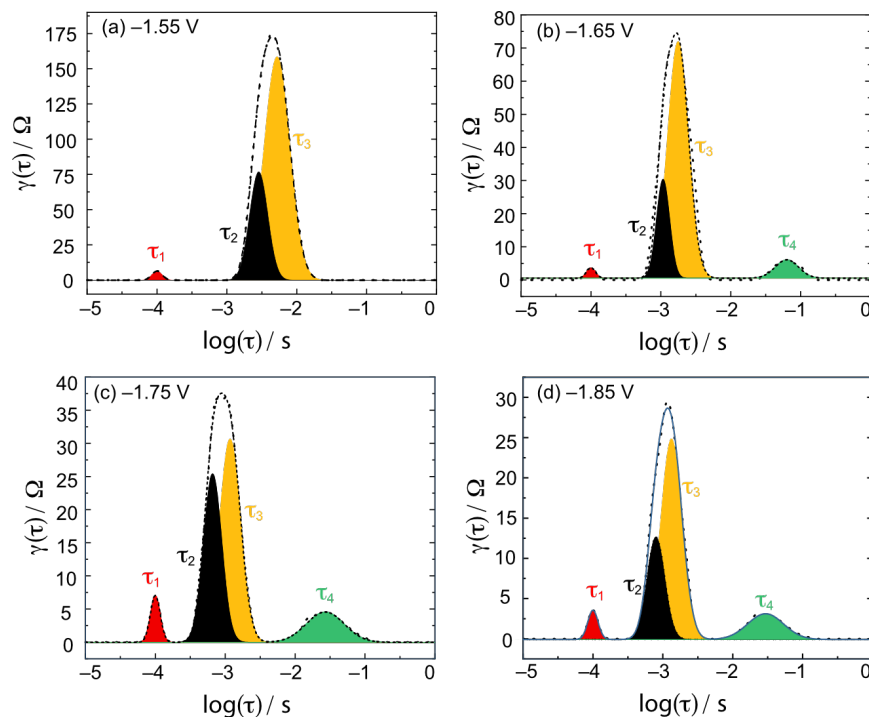


Figure 7. Potential Dependent DRT plots calculated for the 70:30 AgSnO_x composite film electrode measured at various potentials in CO₂ saturated MeCN containing 100 mM [TBA]PF₆ and 100 mM [DBU-H]PF₆. The colors represent relaxation events with different time constants that contribute to overall impedance during CO₂ reduction: τ_1 (red) - Ohmic contact between the thin film and the nickel substrate; τ_2 (black) - Adsorption of IL and related intermediates; τ_3 (yellow) - Charge transfer kinetics and τ_4 (green) diffusion/capacitive behavior related to mass transport.

Table 5. Resistance parameters extracted from the DRT plots in Figure 6 corresponding to the kinetics of CO₂RR on the 70:30 AgSnO_x composite film as a function of applied potential (E_{app}).

E_{app} vs. Ag/AgCl	τ_1	τ_2	τ_3	τ_4
	$R_1 (\Omega)$	$R_2 (\Omega)$	$R_3 (\Omega)$	$R_4 (\Omega)$
-1.55 V	4.5	75	160	—
-1.65 V	4.5	90	70	24
-1.75 V	6.5	25	31	12.5
-1.85 V	7.5	9	23	2.5

shift to shorter times (Figure 7 and Table 5) suggesting that the events become faster. Likewise, the associated resistances of τ_2 and τ_3 decrease as the applied potentials become more negative consistent with more favorable CO₂RR kinetics as the overpotential for electrocatalysis is increased. Both τ_2 and τ_3 directly relate contributions of the heterogenous electron transfer kinetics to the overall resistance of CO₂ reduction. Since these events are directly connected to the potential dependent CO₂ reduction kinetics, the contribution to the total resistance is expected to be potential dependent as well. As shown in Figure 7 and Table 5, the resistances associated with these relaxation processes do indeed decrease at more negative potentials.

Lastly, the broad time constant τ_4 may be attributed to mass transport-controlled polarization resistance during CO₂ reduction and is highly influenced by the diffusion of electrolyte components to the electrode surface as well diffusion of products from the double layer to the bulk solution. As shown by the voltammograms in Figure 4a, for the AgSnO_x electrode of 70:30 composition, potentials more negative than -1.55 V are approximately within the regime of mixed kinetic and diffusion control. As would be expected for a reaction under mass transport control, the associated resistance (τ_4) reaches a maximum value at an applied potential that is ~ 200 mV past the foot of the electrocatalytic wave (*i.e.*, $E_{app} = -1.65$ V for 70:30 AgSnO_x) and decreases further as the applied potential is raised further (See Figure 6 and Table 5).⁶⁰

The 70:30 AgSn composite film exhibits decreased contribution of the diffusion-controlled polarization resistance to the overall resistance, which agrees well with the faster kinetics of CO₂RR observed for these films. This film composition also exhibits a lower onset potential for

CO₂RR in the presence of [DBU-H]⁺. The decreased overall contribution of the charge transfer resistance to the total polarization resistance might also indicate higher electrical conductivity of the thin films upon alloying as has been observed for PbO₂ that had been alloyed with Bi and/or Sn.⁶¹ Although metal oxide derived cathodes have been shown to be highly active and selective for electrocatalytic CO₂ reduction, they are not always highly conductive due to ohmic interparticle resistances, which can compromise the intrinsic electrokinetics of such platforms.⁶ Nonetheless, the overall surface composition is also expected to control the selectivity and electrokinetics of CO₂ reduction on the metal oxides under study.^{6,62,63}

The collection of electroanalytical investigations that have been presented herein support the notion that synergistic interaction between Ag and SnO_x give rise to rough films that support enhanced CO₂RR kinetics. Interestingly, inspection of the distribution of relaxation times also indicates that upon combining Ag with SnO_x, the relaxation times for the events associated with the adsorption-controlled charge transfer events shift to larger relaxation times (*i.e.*, higher frequencies) whereas the relaxation events associated with the diffusion-controlled charge transfer kinetics do not exhibit a significant relaxation time shift. These observations are consistent with the notion that mixing of Ag with SnO_x enhances the efficacy of adsorption and stabilization of reduced CO₂ intermediates and [DBU-H]⁺ cations to facilitate CO evolution at the cathode/electrolyte interface.

CONCLUSIONS AND FUTURE DIRECTIONS

Both Ag- and Sn-based materials have been previously considered as CO₂ reduction catalysts that may offer practical benefits for the sustainable production of carbon-based fuels and commodity chemicals. In this work, we have considered electrodeposited Ag-only, Sn-only, and AgSnO_x composite film electrodes prepared from electroplating baths with varying ratios of Ag⁺ and Sn²⁺ triflates to understand how the performance of such composite materials varies as a function of composition. In particular, the study of electrodeposited AgSnO_x films with varying

ratios of Ag^0 and $\text{Sn}^{2+/4+}$ provided a means to evaluate how the cathode composition impacts CO_2RR electrocatalysis in the presence of $[\text{DBU-H}]^+$ based organic cations within MeCN electrolyte. XPS analysis confirmed that Ag existed in the metallic (Ag^0) state, while the Sn was mainly oxidized ($\text{Sn}^{2+/4+}$) for electrodes that were prepared, including the AgSn composites, which are best considered as AgSnO_x films with varying ratios of $\text{Ag}^0:\text{Sn}^{2+/4+}$.

Evaluation of the AgSnO_x cathodes as electrocatalysts for CO_2RR against the Ag- and Sn-only film electrodes showed the selectivity and efficacy of CO_2 activation varied as function of the $\text{Ag}^0:\text{Sn}^{2+/4+}$ ratios within the films. Consistent with prior work, the Ag-only film was observed to be highly selective for the $2e^-/2\text{H}^+$ reduction of CO_2 to CO, while the Sn-only film produced roughly equal amounts of CO and HCO_2H during CO_2RR electrocatalysis. Much like the Sn-only cathode, composite films that were rich in Sn relative to Ag showed poor selectivities for reduction of CO_2 to CO over production of HCO_2H . However, composite films that had roughly equal levels of $\text{Ag}^0:\text{Sn}^{2+/4+}$ were 85% selective for reduction of CO_2 to CO demonstrating that relatively high current efficiencies for CO evolution could be achieved while cutting the amount of expensive silver in the cathodes in half. Going further, the composite cathode containing roughly twice as much silver as compared to tin, supported CO_2RR catalysis that was slightly better than that observed for the Ag-only electrode. More specifically, the AgSnO_x ($70\text{Ag}^0 : 30\text{Sn}^{2+/4+}$) composite electrode was observed to evolve CO with near quantitative current efficiency and current densities of $\sim 26 \text{ mA/cm}^2$, which slightly higher than that observed for the Ag-only cathode. Accordingly, this work has demonstrated that mixed-metal CO evolution electrocatalysts can be easily electrodeposited from plating solutions and can support metrics typically observed for Ag (and other precious metals), while substituting a significant amount of the precious coinage metal for inexpensive tin.

Electrochemical impedance spectroscopy (EIS) coupled with analysis of the distribution of relaxation times (DRT) was used to evaluate the factors important to the function of the film electrodes considered in this study. Importantly, these analyses showed that adsorption and

diffusion controlled processes are important to the activity of the CO₂RR electrocatalysts that were subjected to EIS and also provided some insights as to the enhanced performance of the AgSnO_x (7 Ag⁰ : 3 Sn^{2+/4+}) composite. The best performing AgSnO_x (7 Ag⁰ : 3 Sn^{2+/4+}) composite was found to exhibit decreased contributions of diffusion-controlled polarization to the overall resistance, which is consistent with the more facile CO₂ reduction kinetics observed for these films. This composite film containing a 7:3 ratio of Ag⁰ : Sn^{2+/4+} also exhibited a lower onset potential for CO₂RR in the presence of [DBU-H]⁺ as compared to the other film electrodes evaluated in this work.

The collection of electroanalytical investigations that we report suggest that synergistic interaction between Ag and SnO_x give rise to rough films that support enhanced CO₂RR kinetics and that mixing of Ag with SnO_x enhances the efficacy of adsorption and stabilization of reduced CO₂ intermediates and electrolyte (*i.e.*, [DBU-H]⁺) cations to facilitate CO evolution at the cathode/electrolyte interface. In addition to pointing to potential strategies to reduce the loading of precious metals (*i.e.*, Ag) in electrocatalysts materials while maintaining exceptional selectivities and high activities for CO evolution, this work also demonstrates how DRT analysis can be leveraged to help analyze EIS data recorded under CO₂RR conditions. Accordingly, the detailed physicochemical origin of the DRT relaxation processes for AgSnO_x and other composite electrocatalyst systems continues to be a point of interest within our laboratory.

ACKNOWLEDGEMENTS

The authors thank L. Xiong for helpful discussions. This work was supported by funding provided by the University of Delaware. Faradaic efficiencies were determined using instrumentation obtained through NSF CHE1352120.

ASSOCIATED CONTENT

Supporting Information: This material is available free of charge via the Internet at <http://pubs.acs.org>.

AUTHOR INFORMATION

Corresponding Author: *E-mail: joelr@udel.edu. Tel: 302-831-0716

Author Contributions: TK and JR contributed equally to the design and writing of the manuscript. TK conducted all experimental work described herein. AA contributed to discussions that spurred the undertaking of this project.

Notes: The authors declare no conflicts of interest.

REFERENCES

- (1) Mota, F. M.; Kim, D. H. From CO₂ Methanation to Ambitious Long-Chain Hydrocarbons: Alternative Fuels Paving the Path to Sustainability. *Chem. Soc. Rev.* **2019**, *48* (1), 205–259.
- (2) Lewis, N. S.; Nocera, D. G. *Powering the Planet: Chemical Challenges in Solar Energy Utilization*; 2006; Vol. 103, pp 15729–15735.
- (3) Durst, J.; Rudnev, A.; Dutta, A.; Fu, Y.; Herranz, J.; Kaliginedi, V.; Kuzume, A.; Permyakova, A. A.; Paratcha, Y.; Broekmann, P.; et al. Electrochemical CO₂ Reduction - A Critical View on Fundamentals, Materials and Applications. *Chimia (Aarau)*. **2015**, *69* (12), 769–776.
- (4) Zhang, L.; Zhao, Z.-J.; Gong, J. Nanostructured Materials for Heterogeneous Electrocatalytic CO₂ Reduction and Their Related Reaction Mechanisms. *Angew. Chemie Int. Ed.* **2017**, *56* (38), 11326–11353.
- (5) Hori, Y. Electrochemical CO₂ Reduction on Metal Electrodes. In *Modern Aspects of Electrochemistry*; Springer New York: New York, NY, 2008; Vol. 42, pp 89–189.
- (6) Garg, S.; Li, M.; Weber, A. Z.; Ge, L.; Li, L.; Rudolph, V.; Wang, G.; Rufford, T. E. Advances and Challenges in Electrochemical CO₂ Reduction Processes: An Engineering and Design Perspective Looking beyond New Catalyst Materials. *J. Mater. Chem. A* **2020**, *8* (4), 1511–1544.
- (7) Feaster, J. T.; Shi, C.; Cave, E. R.; Hatsukade, T.; Abram, D. N.; Kuhl, K. P.; Hahn, C.; Nørskov, J. K.; Jaramillo, T. F. Understanding Selectivity for the Electrochemical Reduction of Carbon Dioxide to Formic Acid and Carbon Monoxide on Metal Electrodes. *ACS Catal.* **2017**, *7* (7), 4822–4827.
- (8) Agarwal, A. S.; Rode, E.; Sridhar, N.; Hill, D. Conversion of CO₂ to Value-Added Chemicals: Opportunities and Challenges. In *Handbook of Climate Change Mitigation and Adaptation*; Springer New York: New York, NY, 2015; pp 1–40.
- (9) Pan, F.; Yang, Y. Designing CO₂reduction Electrode Materials by Morphology and Interface Engineering. *Energy Environ. Sci.* **2020**, *13* (8), 2275–2309.
- (10) Hapiot, P.; Lagrost, C. Electrochemical Reactivity in Room-Temperature Ionic Liquids. *Chem. Rev.* **2008**, *108* (7), 2238–2264.
- (11) Silvester, D. S.; Compton, R. G. Electrochemistry in Room Temperature Ionic Liquids: A

- Review and Some Possible Applications. *Zeitschrift fur Phys. Chemie* **2006**, *220* (10–11), 1247–1274.
- (12) Chen, Y.; Mu, T. Conversion of CO₂ to Value-Added Products Mediated by Ionic Liquids. *Green Chem.* **2019**, *21* (10), 2544–2574.
 - (13) Dimeglio, J. L.; Rosenthal, J. Selective Conversion of CO₂ to CO with High Efficiency Using an Inexpensive Bismuth-Based Electrocatalyst. *J. Am. Chem. Soc.* **2013**, *135* (24), 8798–8801.
 - (14) Medina-Ramos, J.; Pupillo, R. C.; Keane, T. P.; DiMeglio, J. L.; Rosenthal, J. Efficient Conversion of CO₂ to CO Using Tin and Other Inexpensive and Easily Prepared Post-Transition Metal Catalysts. *J. Am. Chem. Soc.* **2015**, *137* (15), 5021–5027.
 - (15) Kunene, T.; Atifi, A.; Rosenthal, J. Selective CO₂ Reduction over Rose's Metal in the Presence of an Imidazolium Ionic Liquid Electrolyte. *ACS Appl. Energy Mater.* **2020**, *3* (5), 4193–4200.
 - (16) Greaves, T. L.; Drummond, C. J. Protic Ionic Liquids: Evolving Structure–Property Relationships and Expanding Applications. *Chem. Rev.* **2015**, *115* (20), 11379–11448.
 - (17) Amarasekara, A. S. Acidic Ionic Liquids. *Chem. Rev.* **2016**, *116* (10), 6133–6183.
 - (18) Greaves, T. L.; Drummond, C. J. Protic Ionic Liquids: Properties and Applications. *Chem. Rev.* **2008**, *108* (1), 206–237.
 - (19) Zeng, X.; Wang, Z.; Rehman, A. Electrode–Electrolyte Interfacial Processes in Ionic Liquids and Sensor Applications. In *Electrochemistry in Ionic Liquids*; Springer International Publishing: Cham, 2015; pp 7–74.
 - (20) Torriero, A. A. J. *Electrochemistry in Ionic Liquids: Volume 2: Applications*; Springer International Publishing, 2015.
 - (21) Lim, H. K.; Kim, H. The Mechanism of Room-Temperature Ionic-Liquid-Based Electrochemical CO₂ Reduction: A Review. *Molecules* **2017**, *22* (4), 536.
 - (22) Faggion, D.; Gonçalves, W. D. G.; Dupont, J. CO₂ Electroreduction in Ionic Liquids. *Front. Chem.* **2019**, *7* (MAR), 102.
 - (23) Atifi, A.; Boyce, D. W.; Dimeglio, J. L.; Rosenthal, J. Directing the Outcome of CO₂ Reduction at Bismuth Cathodes Using Varied Ionic Liquid Promoters. *ACS Catal.* **2018**, *8* (4), 2857–2863.
 - (24) Rahman, M. H.; Atifi, A.; Rosenthal, J.; Ryan, M. D. Reversible Proton-Coupled Reduction of an Iron Nitrosyl Porphyrin within [DBU–H]⁺-Based Protic Ionic Liquid Nanodomains. *Inorg. Chem.* **2021**.
 - (25) Mahyoub, S. A.; Qaraah, F. A.; Chen, C.; Zhang, F.; Yan, S.; Cheng, Z. An Overview on the Recent Developments of Ag-Based Electrodes in the Electrochemical Reduction of CO₂ to CO. *Sustain. Energy Fuels* **2020**, *4* (1), 50–67.
 - (26) Leung, K. Y.; McCrory, C. C. L. Effect and Prevention of Trace Ag⁺ Contamination from Ag/AgCl Reference Electrodes on CO₂ Reduction Product Distributions at Polycrystalline Copper Electrodes. *ACS Appl. Energy Mater.* **2019**, *2* (11), 8283–8293.
 - (27) Cho, M.; Seo, J. W.; Song, J. T.; Lee, J. Y.; Oh, J. Silver Nanowire/Carbon Sheet Composites for Electrochemical Syngas Generation with Tunable H₂/CO Ratios. *ACS Omega* **2017**, *2* (7), 3441–3446.
 - (28) Zhao, S.; Li, S.; Guo, T.; Zhang, S.; Wang, J.; Wu, Y.; Chen, Y. Advances in Sn-Based Catalysts for Electrochemical CO₂ Reduction. *Nano-Micro Lett.* **2019**, *11* (1), 62.
 - (29) Hori, Y.; Wakebe, H.; Tsukamoto, T.; Koga, O. Electrocatalytic Process of CO Selectivity in Electrochemical Reduction of CO₂ at Metal Electrodes in Aqueous Media. *Electrochim. Acta* **1994**, *39* (11–12), 1833–1839.
 - (30) Bumroongsakulsawat, P.; Kelsall, G. H. Effect of Solution PH on CO: Formate Formation Rates during Electrochemical Reduction of Aqueous CO₂ at Sn Cathodes. *Electrochim. Acta* **2014**, *141*, 216–225.
 - (31) König, M.; Vaes, J.; Klemm, E.; Pant, D. Solvents and Supporting Electrolytes in the

- Electrocatalytic Reduction of CO₂. *iScience* **2019**, *19*, 135–160.
- (32) Wang, Y.; Liu, J.; Wang, Y.; Al-Enizi, A. M.; Zheng, G. Tuning of CO₂ Reduction Selectivity on Metal Electrocatalysts. *Small* **2017**, *13* (43).
- (33) Al-Rowaili, F. N.; Jamal, A.; Ba Shammakh, M. S.; Rana, A. A Review on Recent Advances for Electrochemical Reduction of Carbon Dioxide to Methanol Using Metal-Organic Framework (MOF) and Non-MOF Catalysts: Challenges and Future Prospects. *ACS Sustain. Chem. Eng.* **2018**, *6* (12), 15895–15914.
- (34) Chen, Z.; Vannucci, A. K.; Concepcion, J. J.; Jurss, J. W.; Meyer, T. J. Proton-Coupled Electron Transfer at Modified Electrodes by Multiple Pathways. *Proc. Natl. Acad. Sci. U. S. A.* **2011**, *108* (52), E1461–E1469.
- (35) Taifan, W.; Boily, J. F.; Baltrusaitis, J. Surface Chemistry of Carbon Dioxide Revisited. *Surf. Sci. Rep.* **2016**, *71* (4), 595–671.
- (36) Pander, J. E.; Ren, D.; Huang, Y.; Loo, N. W. X.; Hong, S. H. L.; Yeo, B. S. Understanding the Heterogeneous Electrocatalytic Reduction of Carbon Dioxide on Oxide-Derived Catalysts. *ChemElectroChem* **2018**, *5* (2), 219–237.
- (37) Luc, W.; Collins, C.; Wang, S.; Xin, H.; He, K.; Kang, Y.; Jiao, F. Ag-Sn Bimetallic Catalyst with a Core-Shell Structure for CO₂ Reduction. *J. Am. Chem. Soc.* **2017**, *139* (5), 1885–1893.
- (38) Sun, Z.; Ma, T.; Tao, H.; Fan, Q.; Han, B. Fundamentals and Challenges of Electrochemical CO₂ Reduction Using Two-Dimensional Materials. *Chem* **2017**, *3* (4), 560–587.
- (39) Chen, Y.; Kanan, M. W. Tin Oxide Dependence of the CO₂ Reduction Efficiency on Tin Electrodes and Enhanced Activity for Tin/Tin Oxide Thin-Film Catalysts. *J. Am. Chem. Soc.* **2012**, *134* (4), 1986–1989.
- (40) Dutta, A.; Kuzume, A.; Rahaman, M.; Veszteg, S.; Broekmann, P. Monitoring the Chemical State of Catalysts for CO₂ Electroreduction: An In Operando Study. *ACS Catal.* **2015**, *5* (12), 7498–7502.
- (41) Pander, J. E.; Baruch, M. F.; Bocarsly, A. B. Probing the Mechanism of Aqueous CO₂ Reduction on Post-Transition-Metal Electrodes Using ATR-IR Spectroelectrochemistry. *ACS Catal.* **2016**, *6* (11), 7824–7833.
- (42) Choi, Y.-W. W.; Scholten, F.; Sinev, I.; Cuenya, B. R.; Roldan Cuenya, B. Enhanced Stability and CO/Formate Selectivity of Plasma-Treated SnO_x/AgO_x Catalysts during CO₂ Electroreduction. *J. Am. Chem. Soc.* **2019**, *141* (13), 5261–5266.
- (43) Yoon, Y.; Yan, B.; Surendranath, Y. Suppressing Ion Transfer Enables Versatile Measurements of Electrochemical Surface Area for Intrinsic Activity Comparisons. *J. Am. Chem. Soc.* **2018**, *140* (7), 2397–2400.
- (44) Wei, C.; Sun, S.; Mandler, D.; Wang, X.; Qiao, S. Z.; Xu, Z. J. Approaches for Measuring the Surface Areas of Metal Oxide Electrocatalysts for Determining Their Intrinsic Electrocatalytic Activity. *Chem. Soc. Rev.* **2019**, *48* (9), 2518–2534.
- (45) Connor, P.; Schuch, J.; Kaiser, B.; Jaegermann, W. The Determination of Electrochemical Active Surface Area and Specific Capacity Revisited for the System MnO_x as an Oxygen Evolution Catalyst. *Zeitschrift fur Phys. Chemie* **2020**, *234* (5), 979–994.
- (46) Wan, T. H.; Saccoccio, M.; Chen, C.; Ciucci, F. Influence of the Discretization Methods on the Distribution of Relaxation Times Deconvolution: Implementing Radial Basis Functions with DRTtools. *Electrochim. Acta* **2015**, *184*, 483–499.
- (47) IAM - Karlsruhe Institute of Technology. Lin-KK tool <http://www.iam.kit.edu/wet/Lin-KK.php> (accessed May 9, 2020).
- (48) Schönleber, M.; Klotz, D.; Ivers-Tiffée, E. A Method for Improving the Robustness of Linear Kramers-Kronig Validity Tests. *Electrochim. Acta* **2014**, *131*, 20–27.
- (49) Schönleber, M.; Ivers-Tiffée, E. Approximability of Impedance Spectra by RC Elements

- and Implications for Impedance Analysis. *Electrochem. commun.* **2015**, *58*, 15–19.
- (50) Moulder, J. F.; Stickle, W. F.; Sobol, P. E.; Bomben, K. D. *Handbook of X-Ray Photoelectron Spectroscopy: A Reference Book of Standard Spectra for Identification and Interpretation of XPS Data*; Chastain, J., Ed.; Perkin-Elmer Corporation, 1992.
- (51) Karakaya, I.; Thompson, W. T. The Ag-Sn (Silver-Tin) System. *Bull. Alloy Phase Diagrams* **1987**, *8* (4), 340–347.
- (52) *Alloy Phase Diagrams*; Okamoto, H., Schlesinger, M. E., Mueller, E. M., Eds.; ASM International, 2016.
- (53) Walsh, F. C.; Low, C. T. J. A Review of Developments in the Electrodeposition of Tin-Copper Alloys. *Surface and Coatings Technology*. 2016, pp 246–262.
- (54) Wu, J.; Risalvato, F. G.; Ma, S.; Zhou, X. D. Electrochemical Reduction of Carbon Dioxide III. the Role of Oxide Layer Thickness on the Performance of Sn Electrode in a Full Electrochemical Cell. *J. Mater. Chem. A* **2014**, *2* (6), 1647–1651.
- (55) Zhang, R.; Lv, W.; Lei, L. Role of the Oxide Layer on Sn Electrode in Electrochemical Reduction of CO₂ to Formate. *Appl. Surf. Sci.* **2015**, *356*, 24–29.
- (56) Schichlein, H.; Müller, A. C.; Voigts, M.; Krügel, A.; Ivers-Tiffée, E. Deconvolution of Electrochemical Impedance Spectra for the Identification of Electrode Reaction Mechanisms in Solid Oxide Fuel Cells. *J. Appl. Electrochem.* **2002**, *32* (8), 875–882.
- (57) Ciucci, F. Modeling Electrochemical Impedance Spectroscopy. *Curr. Opin. Electrochem.* **2019**, *13*, 132–139.
- (58) Choi, W.; Shin, H. C.; Kim, J. M.; Choi, J. Y.; Yoon, W. S. Modeling and Applications of Electrochemical Impedance Spectroscopy (Eis) for Lithium-Ion Batteries. *J. Electrochem. Sci. Technol.* **2020**, *11* (1), 1–13.
- (59) Dhillon, S.; Kant, R. Theory for Electrochemical Impedance Spectroscopy of Heterogeneous Electrode with Distributed Capacitance and Charge Transfer Resistance. *J. Chem. Sci.* **2017**, *129* (8), 1277–1292.
- (60) Lasia, A. Impedance of the Faradaic Reactions in the Presence of Mass Transfer. In *Electrochemical Impedance Spectroscopy and its Applications*; Springer New York, 2014; pp 85–125.
- (61) Choi, S. Y.; Jeong, S. K.; Kim, H. J.; Baek, I. H.; Park, K. T. Electrochemical Reduction of Carbon Dioxide to Formate on Tin-Lead Alloys. *ACS Sustain. Chem. Eng.* **2016**, *4* (3), 1311–1318.
- (62) Ma, M.; Trześniewski, B. J.; Xie, J.; Smith, W. A. Selective and Efficient Reduction of Carbon Dioxide to Carbon Monoxide on Oxide-Derived Nanostructured Silver Electrocatalysts. *Angew. Chemie Int. Ed.* **2016**, *55* (33), 9748–9752.
- (63) Lum, Y.; Yue, B.; Lobaccaro, P.; Bell, A. T.; Ager, J. W. Optimizing C-C Coupling on Oxide-Derived Copper Catalysts for Electrochemical CO₂ Reduction. *J. Phys. Chem. C* **2017**, *121* (26), 14191–14203.

TOC Graphic

